Environmental Pollution 195 (2014) 282–291

Contents lists available at ScienceDirect

Environmental Pollution

journal homepage: www.elsevier.com/locate/envpol

Factors influencing surface CO_2 variations in LPRU, Thailand and IESM, Philippines

Ronald Macatangay [a, b, *], Thiranan Sonkaew [c], Voltaire Velazco [d], Christoph Gerbig [e], Nilubol Intarat [c], Nittaya Nantajai [c], Gerry Bagtasa [a, b]

[a] Institute of Environmental Science and Meteorology, University of the Philippines, Diliman, Quezon City, Philippines
[b] Natural Sciences Research Institute, University of the Philippines, Diliman, Quezon City, Philippines
[c] Science Faculty, Lampang Rajabhat University, Lampang, Thailand
[d] Centre for Atmospheric Chemistry, University of Wollongong, Australia
[e] Max Planck Institute for Biogeochemistry, Hans-Knöll-Str.10, 07745 Jena, Germany

A R T I C L E I N F O

Article history:
Received 10 February 2014
Received in revised form
7 June 2014
Accepted 28 June 2014
Available online 21 July 2014

Keywords:
Carbon dioxide
Non-dispersive infrared
Multiple linear regression
Regression coefficients
Lagrangian transport model
Backtrajectory
Footprints

A B S T R A C T

Surface carbon dioxide concentrations were measured using a non-dispersive infrared carbon dioxide sensor at Lampang Rajabhat University from April to May 2013 and at the University of the Philippines-Diliman campus starting September 2013. Factors influencing the variations in these measurements were determined using multiple linear regression and a Lagrangian transport model. Air temperature and sea level pressure were the dominant meteorological factors that affect the CO_2 variations. However, these factors are not enough. Surface CO_2 flux and transboundary transport needs to be considered as well.

1. Introduction

Global temperature is rising. This is a known fact. The Intergovernmental Panel on Climate Change (IPCC) have proven this time and again in their previous assessment reports as well as in their newest report released in 2013. Together with this temperature increase comes sea-level rise. In IPCC's 2013 report, four scenarios of carbon emissions were presented. These were termed as Representative Concentration Pathways (RCPs) that drive the temperature and sea-level scenarios. According to these RCPs, temperatures will rise by as much as 2 °C if we stop carbon emissions by 2020 and will increase by 4 °C for business as usual carbon emissions by 2100. This translates to a sea-level rise increase of approximately 0.5 m and 1.0 m, respectively (IPCC et al., 2012). This makes communities in Southeast Asia, particularly cities such as Ho Chi Minh, Jakarta, Bangkok, Manila and Yangon, more vulnerable (Potsdam Institute of Climate Research and Climate Analytics (2013)). Since almost half of the anthropogenic carbon emissions remain in the atmosphere, continuous measurements of atmospheric carbon dioxide (CO_2) concentrations are therefore essential.

Information about carbon dioxide concentrations spans different scales and platforms. One can look at the global scale using satellites (e.g. SCIAMACHY, GOSAT) and models (e.g. TM3, CarbonTracker). Regionally, ground-based stations (e.g. TCCON) and nested regional models (e.g. CarbonTraker Asia, STILT) are available. At local scale, in situ measurements can be utilized. However, these platforms are relatively expensive for developing countries such as the Philippines and Thailand. Inexpensive monitoring solutions are therefore essential. Non-dispersive infrared (NDIR) sensors have the potential to provide this inexpensive solution for carbon dioxide concentration monitoring.

Carbon, being one of the basic elements of life, is always on the move, shifting between the atmosphere, the oceans, and the land. Even as plant growth takes large amounts of carbon dioxide out of the air, land-use changes, such as the widespread conversion of forests to agricultural fields add carbon to the atmosphere. Processes in the ocean, including shell formation by marine crustaceans, soak up huge amounts of carbon. Meanwhile, slow geologic processes,

* Corresponding author.
E-mail address: ronmcdo@gmail.com (R. Macatangay).

http://dx.doi.org/10.1016/j.envpol.2014.06.035
0269-7491/

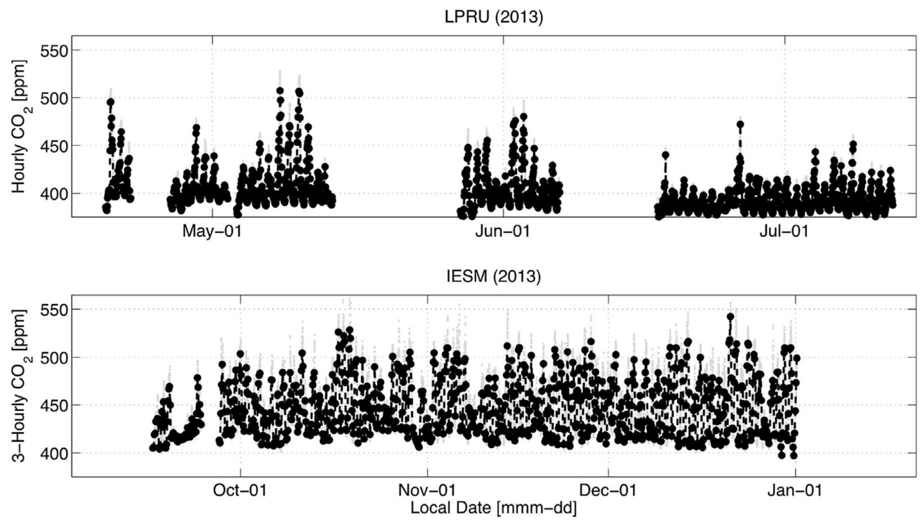

Fig. 1. Surface CO_2 concentration time-series measured at LPRU, Thailand (top) and IESM, Philippines (bottom).

like coal or natural gas formation, sequester large amounts of carbon underground. However, mankind has learned how to harness this fossil fuel, releasing a large amount of carbon into the atmosphere. Only about 40% of the carbon that we are emitting stays in the atmosphere, and the remaining 60% are being taken up by the world's oceans and land plants. We don't really know where on land this carbon is being taken up. Computer models for a long time have indicated that a large amount of CO_2 is coming out of the tropics possibly as a result of deforestation and a large amount is being taken up in the northern forests in the U.S., in Europe, in Canada and Russia. However, researchers on the ground looking for that carbon in the north were not able to find it. This is sometimes referred to as the *missing carbon sink*. It has been found that more CO_2 is taken up by tropical forests than what was previously thought and less CO_2 is being taken up by northern forests (Stephens et al., 2007). This stresses the importance of carbon dioxide measurements in tropical regions for understanding carbon source/sink processes (tropical rainforest deforestation, tropical reservoir out gassing, etc.).

There is a lot of uncertainty in carbon emissions in the tropics. Monitoring surface CO_2 concentrations in this region is therefore essential. However, most countries in the tropics are poor or developing nations. This limits capabilities of extensive atmospheric carbon dioxide measurements in this region. Low-cost solutions for CO_2 monitoring are needed. NDIR sensors offer the solution for moderate accuracy with inexpensive carbon dioxide measurements. The Berkeley Atmospheric CO_2 Observation Network, or BEACO$_2$N, has proven that "*instead of using a small number of extremely sensitive instruments to measure a large area, interesting locations are blanketed with a high density network of moderate quality instruments, that when taken together as a network produce an accurate, highly resolved picture of real-time CO_2 concentrations*" (http://beacon.berkeley.edu/). In this light, this study aimed at determining the factors influencing surface CO_2 concentrations using a single low-cost and moderate accuracy NDIR sensor in synergy with multiple linear regression and a Lagrangian transport model.

2. Methodology

A low-cost, moderate accuracy NDIR sensor was used in this study. It works using a diffusion sampling method with a 20 s diffusion time. The overall precision of the sensor is ±1 ppm and it is calibrated with a 400 ppm CO_2 tank. The operating temperature of the sensor is from 0 to 50 °C and an operating relative humidity

Table 1
List of independent variables, x_{ik}, input to the multiple linear regression for the LPRU and IESM sites.

Independent variables	LPRU	IESM
x_{i1}	Air Temperature [°C]	Air Temperature [°C]
x_{i2}	Sea Level Pressure [hPa]	Sea Level Pressure [hPa]
x_{i3}	Relative Humidity [%]	Relative Humidity [%]
x_{i4}	Wind Speed [km/h]	
x_{i5}	Precipitation [mm]	
x_{i6}	Wind Direction [^{O} from N]	
x_{i7}	Wind Gusts [km/h]	
x_{i8}	Wind Gust Direction [^{O} from N]	

of 0–96%. Additionally, since it is being operated in the tropics, an additional hydrophobic filter was installed. Sampling time may be varied with a minimum of one sample every 2 s.

Surface CO_2 measurements using the NDIR sensor were carried out at Lampang Rajabhat University (LPRU) (18° 13′ 59.47″ N, 99° 29′ 10.24" E, 12 m agl, UTC+7), which is a suburban site in Lampang province in Northern Thailand, and at the Institute of Environmental Science and Meteorology (IESM), University of the Philippines, Diliman campus, Quezon City (14° 38′ 56.76″ N, 121° 4′ 16.32″ E, 12 m agl, UTC+8), which is a highly urbanized site. Surrounding LPRU are numerous rice fields and agricultural land. The measurements at LPRU were performed from April 19 – July 12, 2013 (with April being the peak of biomass burning in the region) as part of a pilot study. Meanwhile, the measurements at IESM are routinely performed starting from September 16, 2013. In this

Table 2
List of regression coefficients, β_k, calculated from the multiple linear regression for the LPRU and IESM sites. Also indicated is the RMS for each site. Bold and italicized are the top-two (in terms of absolute magnitudes and β_0 excluded) regression coefficients for LPRU and IESM.

Regression coefficients	LPRU (RMS = ±16.9477 ppm)	IESM (RMS = ±19.0691 ppm)
β_0	−1040.8	−2185.1
β_1	***−1.9576***	***−4.6680***
β_2	***1.5492***	***2.6697***
β_3	−0.1434	0.7399
β_4	−0.3061	
β_5	−0.0774	
β_6	−0.0111	
β_7	−0.7443	
β_8	−0.0086	

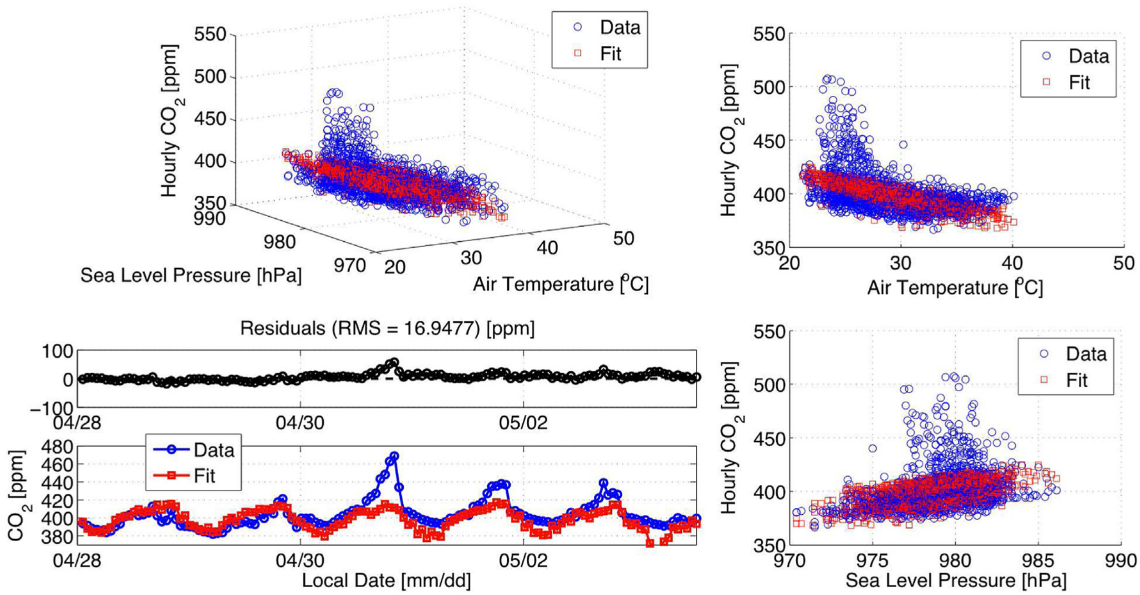

Fig. 2. LPRU Surface CO_2 concentration data and fit (y_i) as a function of the top-two highest regression coefficients in terms of absolute magnitudes (air temperature and sea level pressure).

paper, only up to January 1, 2014 5 AM local time would be presented for the IESM site. The measurements at LPRU were collected every 1-min then averaged to every hour while the data from IESM were measured at 5-min sampling intervals averaged to 3-hourly to match the meteorological data from the local synoptic stations at LPRU and IESM, respectively.

2.1. Meteorological factors

The local meteorological data utilized in the study came from the Thai Meteorological Department (TMD) situated at the Lampang airport (18° 16′ 15.36″ N, 99° 30′ 15″ E) for the LPRU site, and from the Philippine Atmospheric and Geophysical and Astronomical Services Administration (PAGASA) located at the Science Garden in Quezon City (14° 38′ 39″ N, 121° 2′ 39″ E) for the IESM site. In order to determine the contribution of the available meteorological parameters to the measured surface CO_2 concentrations, multiple linear regression was performed.

Multiple linear regression entails relating the dependent variable, y_i, to two or more independent variables, x_{ik}. For k independent variables, its form is given by equation (1)

$$y_i = \beta_0 + \beta_1 x_{i1} + \beta_2 x_{i2} + \ldots + \beta_k x_{ik} + e_i, \quad i = 1, 2, \ldots, n. \tag{1}$$

β_k are called the regression coefficients or least squares estimator, and e_i are the errors. In matrix form, equation (1) simplifies to

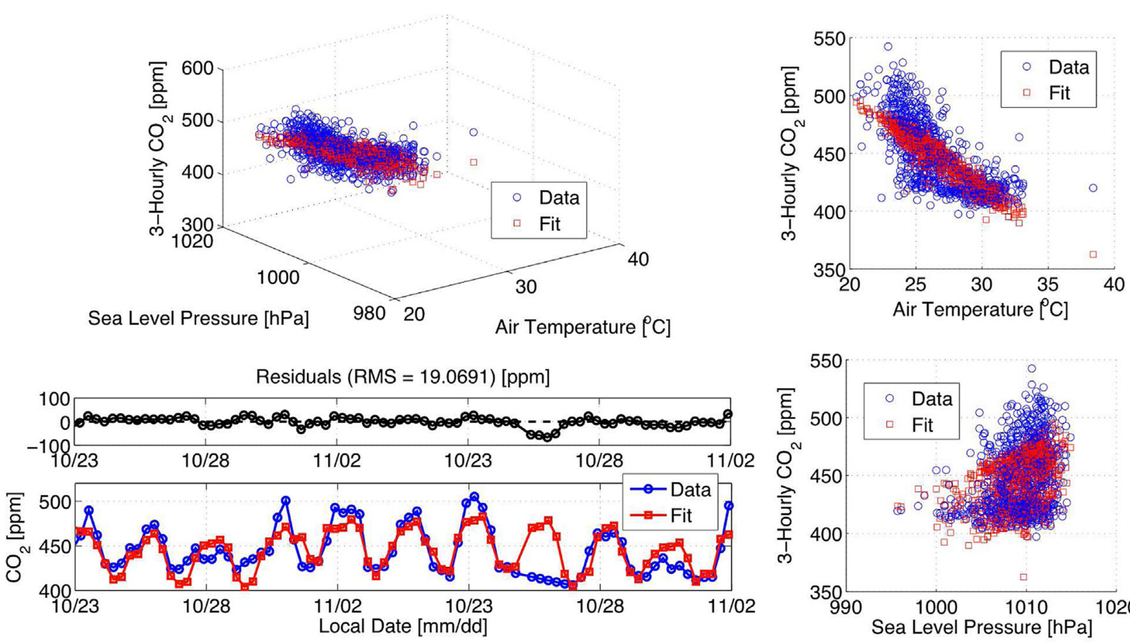

Fig. 3. IESM Surface CO_2 concentration data and fit (y_i) as a function of the top-two highest regression coefficients in terms of absolute magnitudes (air temperature and sea level pressure).

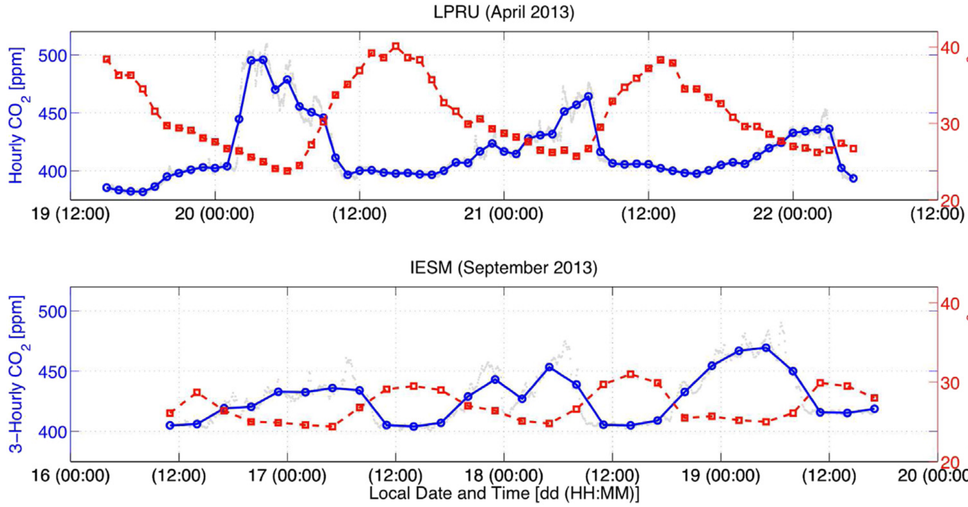

Fig. 4. Diurnal surface CO_2 concentration and air temperature variations during representative dates at the LPRU and IESM sites.

$$Y = X\beta + \varepsilon \tag{2}$$

or explicitly

$$\begin{bmatrix} y_1 \\ y_2 \\ \vdots \\ y_n \end{bmatrix} = \begin{bmatrix} 1 & x_{11} & \dots & x_{1k} \\ 1 & x_{21} & \dots & x_{2k} \\ \vdots & \vdots & \ddots & \vdots \\ 1 & x_{n1} & \dots & x_{nk} \end{bmatrix} \begin{bmatrix} \beta_0 \\ \beta_1 \\ \vdots \\ \beta_k \end{bmatrix} + \begin{bmatrix} \varepsilon_1 \\ \varepsilon_2 \\ \vdots \\ \varepsilon_n \end{bmatrix}. \tag{3}$$

An important requirement of multiple linear regression is that x_{ik}'s are linearly independent. This can be checked by calculating $(X^TX)^{-1}$ if it exists. The least squares estimators can then be calculated using

$$\widehat{\beta} = \left(X^TX\right)^{-1} X^TY. \tag{4}$$

From the regression coefficients, the contribution of each meteorological parameter available can be assessed. The root-mean-square error (RMS) of Y from the data Y_{data} was also calculated as a measure of how well the multiple linear regression model mimics the measured data. This is given by

$$\mathrm{RMS} = \sqrt{\frac{\sum_{i=1}^{n}\left(y_{\mathrm{data},i} - y_i\right)^2}{n}}. \tag{5}$$

2.2. Surface influences (footprints)

Meteorological factors are not the only ones that affect the surface CO_2 concentrations. Depending upon the location of a site, other factors may come into play. One such factor is the surface CO_2 fluxes that maybe transported to the site. For this factor, the Stochastice Time-Inverted Lagrangian Transport (STILT) model (driven by the meteorological fields of the Global Data Assimilation System model) was utilized in this study to infer regions that influence the measurements. This is performed by releasing hypothetical particles backward in time (*backtrajectory*) from the measurement location (*receptor*). After the specified backtrajectory time (3-h at ~1.84 × 2.78 km and 3-days at dynamic horizontal resolution with the smallest horizontal resolution being ~18.4 × 27.8 km horizontal resolution in this study), the particles would land at a volume (specified by z_{bottom} and z_{top}). A volume that receives more

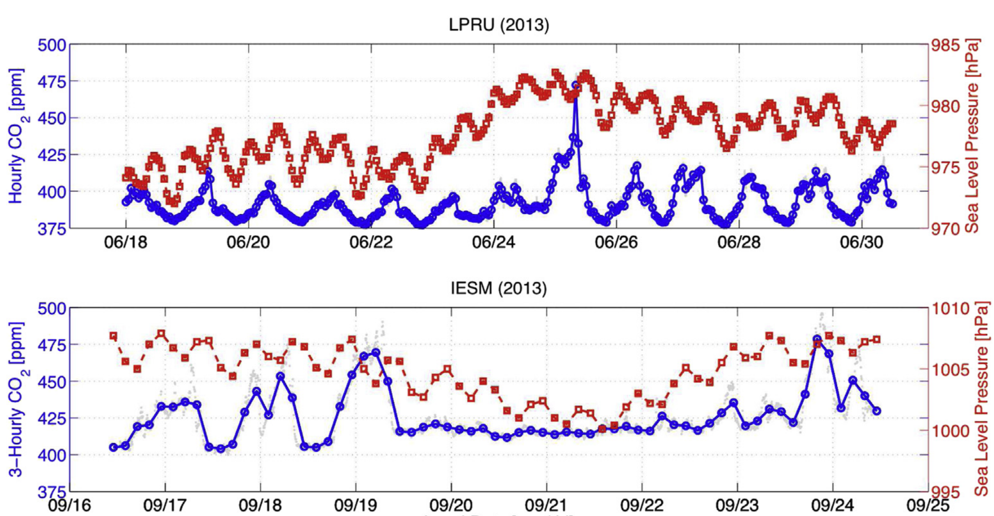

Fig. 5. Effect on the day-to-day variations of surface carbon dioxide concentration amplitudes due to the passage of a high and low pressure systems at the LPRU (upper panel) and IESM (lower panel) sites.

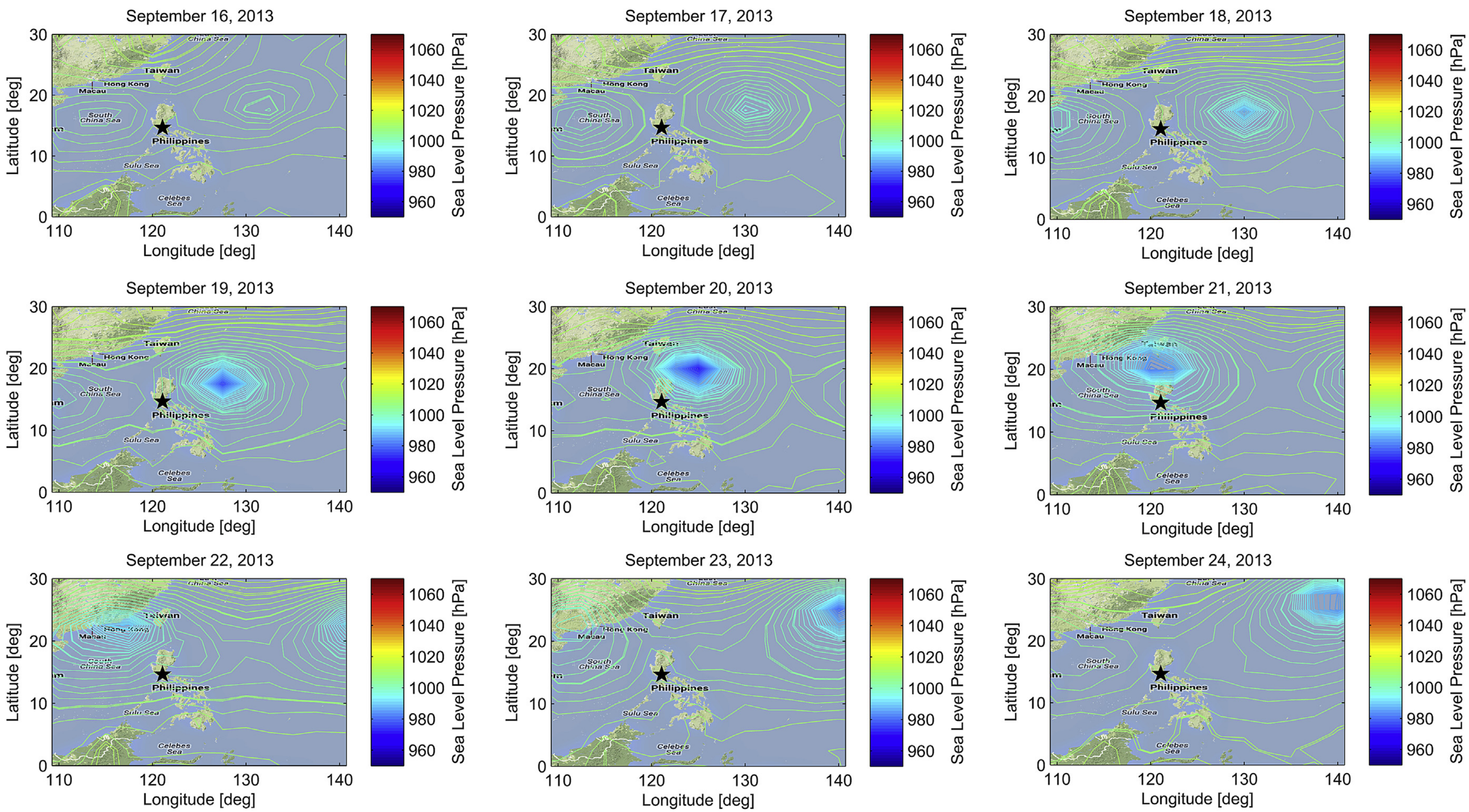

Fig. 6. Sea level pressure fields (provided by NCEP Reanalysis, NOAA/OAR/ESRL PSD, Boulder, Colorado, USA, from their Web site at http://www.esrl.noaa.gov/psd/; Kalnay and Kanamitsu, 1996) as typhoon Usagi (Odette) traverses regions around the Philippines.

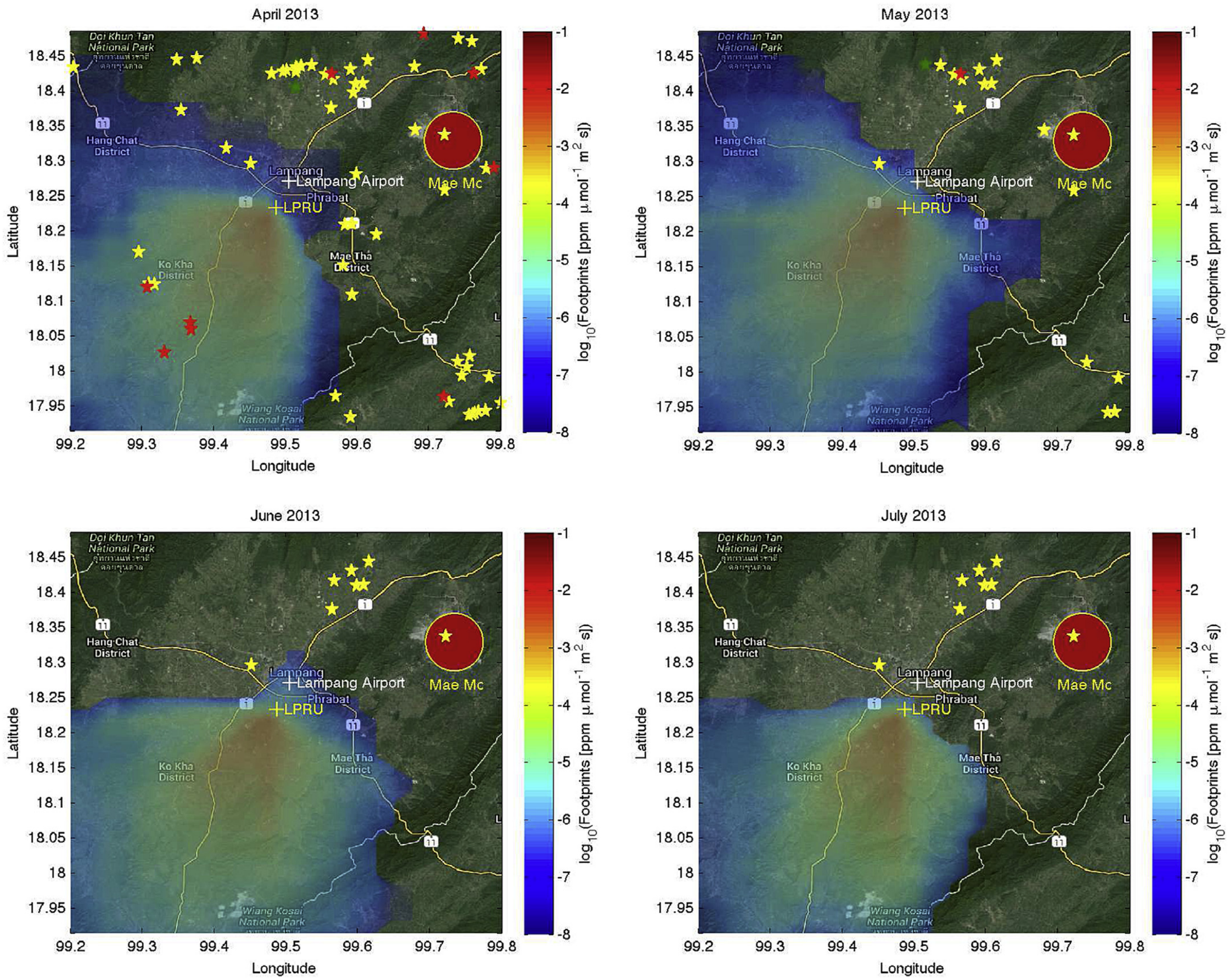

Fig. 7. 3-h backtrajectory footprints for LPRU, Thailand for April, May, June and July 2013. The red circle is Mae Mo coal fired power plant producing 13,606,000 MWh of output energy, emitting 1240 kg of CO_2 per MWh for a total of 16,924,000 tons of CO_2 emissions for the year 2009 (data from CARMA, www.carma.org). Also overlaid as stars are fire hotspots from the Moderate Resolution Imaging Spectroradiometer or MODIS. Green stars indicate 0–30% confidence, yellow stars depict 30–80% confidence and red stars show 80–100% confidence. The number of hourly data for April is $N = 180$, for May is $N = 396$, for June is $N = 470$ while for July is $N = 270$. (For interpretation of the references to colour in this figure legend, the reader is referred to the web version of this article.)

particles, has a greater influence compared to other volumes. The volume can also be made into a surface by setting $z_{\text{bottom}} = z_{\text{top}}$ resulting to *surface influences* or *footprints*, $f(x_i, y_j, t_m)$ in units of ppm μmol^{-1} m^2 s (Gerbig et al., 2003; Lin et al., 2003). The footprints relate surface fluxes, $F(x_i, y_j, t_m)$ (in units of μmol m^{-2} s^{-1}) to changes in concentration, $\Delta c(t_m) = c(t_m) - c_o(t_m)$ (in ppm), at the receptor, where $c_o(t_m)$ is the background concentration.

3. Results

Fig. 1 shows the time-series of the surface CO_2 concentrations measured at LPRU and IESM. The gaps in the data indicate periods when power outages occurred due to weather such as intense thunderstorms or due to electrical problems of the facilities. The length of the time gaps depended upon the availability of the operator to restart the sensor.

Table 1 shows the available independent meteorological variables that were utilized in the multiple linear regression for the LPRU and IESM sites. Due to the availability of data, 8 meteorological parameters were used for LPRU and 3 meteorological fields for IESM.

Indicated in Table 2 are the regression coefficients that were determined in the multiple linear regression for the LPRU and IESM sites.

Figs. 2 and 3 depict scatter plots of the LPRU and IESM surface CO_2 concentration data as a function of the top-two highest regression coefficients of the multiple linear regression in terms of absolute magnitudes (air temperature and sea level pressure for LPRU and IESM), respectively. Also plotted are the fits, y_i, and its time-series calculated from the multiple linear regression.

4. Discussion

4.1. Diurnal variations

Without considering β_0, the dominant regression coefficient, β_1, that is associated with the *air temperature* independent variable, x_{i1} (see Tables 1 and 2). During typical atmospheric pressure conditions, air temperature peaks during the afternoon. The daily maximum temperature generally lags the peak in solar radiation, which normally occurs at noon in the tropics, due to the fact that the heated surface still needs to warm the surrounding atmosphere. Surface warming due to the sun causes thermal plumes to ascend and with it moisture, heat, aerosols and trace gases such as carbon dioxide. This produces strong convection generating intense turbulence, hence deep planetary boundary layer (PBL) mixing. Together with photosynthesis, this produces a minimum in the surface CO_2 concentrations. This is depicted in Fig. 4 for the LPRU and IESM sites. When the sun goes down, solar heating ceases and radiative cooling and surface friction stabilize the lowermost portions of the planetary boundary layer. This results in weak convection producing shallow planetary boundary layer mixing. Hand-in-hand with soil respiration, this causes the maximum in surface carbon dioxide concentration values.

In the case of passages of high pressure systems, this causes a shallower boundary layer due to subsidence and divergence of air parcels. During low pressure conditions, the PBL structure is not that straightforward. Air masses converge in relation to updrafts that are produced. This results in large variation of the boundary layer heights. This gives rise to day-to-day variations of surface CO_2 concentrations.

4.2. Day-to-day variations

As mentioned in the section above, passages of weather systems bring about day-to-day variations in surface carbon dioxide concentrations. This is exemplified by comparing the amplitudes of the surface CO_2 values from June 18–30, 2013 for the LPRU site and from September 16–24, 2013 for the IESM site with the measured sea level pressure as shown in Fig. 5.

For the LPRU site, low pressures of approximately 975 hPa caused low amplitudes of surface CO_2 concentrations during the

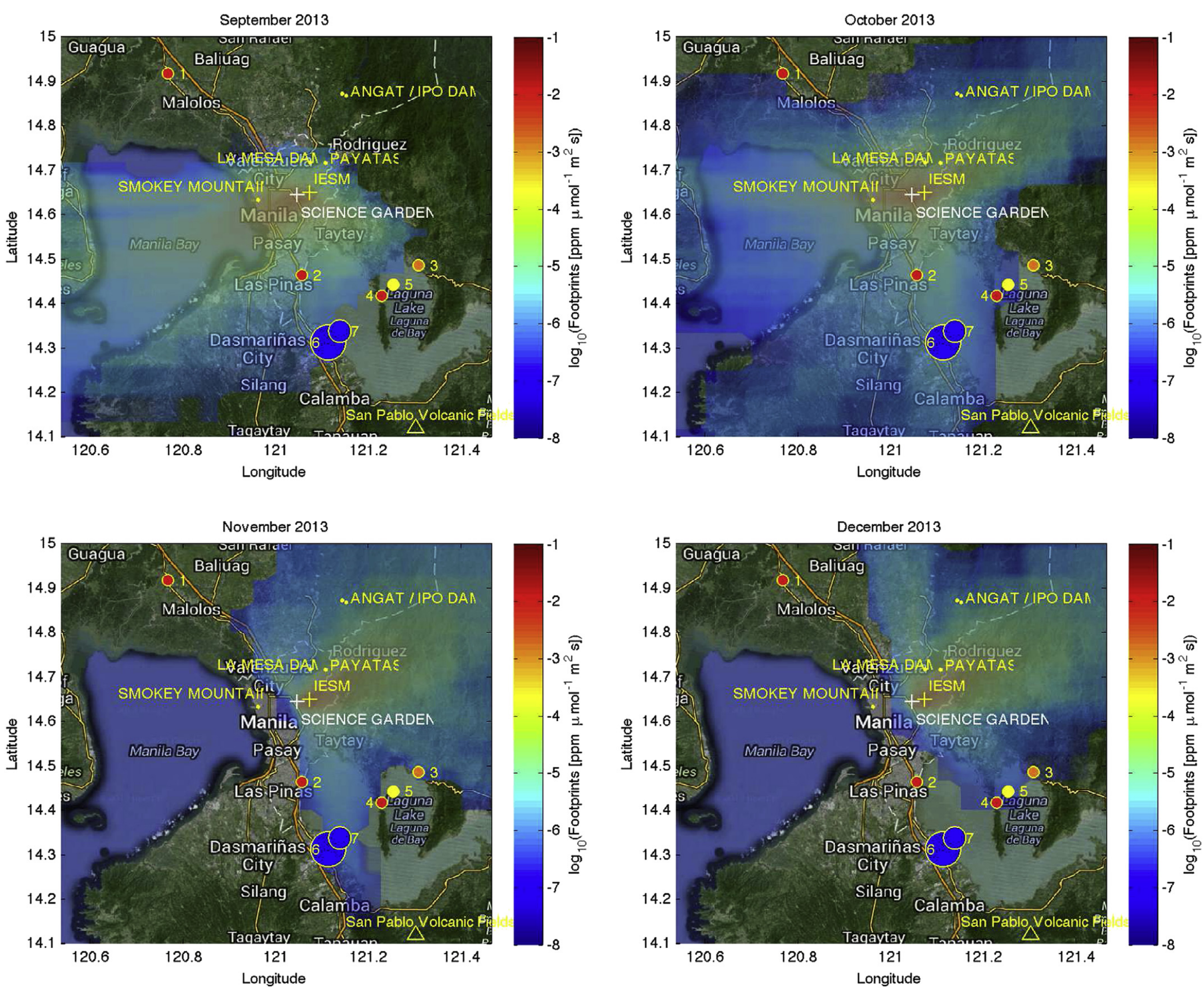

Fig. 8. 3-h backtrajectory footprints for IESM, Philippines for September, October, November and December 2013. The circles are power plants around IESM (1 – Calumpit Mill; 2 – Sucat; 3 – Malaya; 4 – Navotas Barge; 5 – Navotas; 6 – Santa Rita Batangas; 7. San Lorenzo FGP). The size of the circle depends on the output energy while the color indicates the intensity in kilograms of CO_2 per MWh (blue: 150–400; yellow: 400–650; Orange: 650–900; red: >900). The power plant data is for the year 2009 (data from CARMA, www.carma.org). Other potential CO_2 sources are also indicated in the figure (e.g. Angat, Ipo and La Mesa dams, Payatas and Smokey Mountain landfills and San Pablo volcanic fields. The number of 3-hourly data for September is $N = 95$, for October is $N = 244$, for November is $N = 239$ while for December is $N = 248$. (For interpretation of the references to colour in this figure legend, the reader is referred to the web version of this article.)

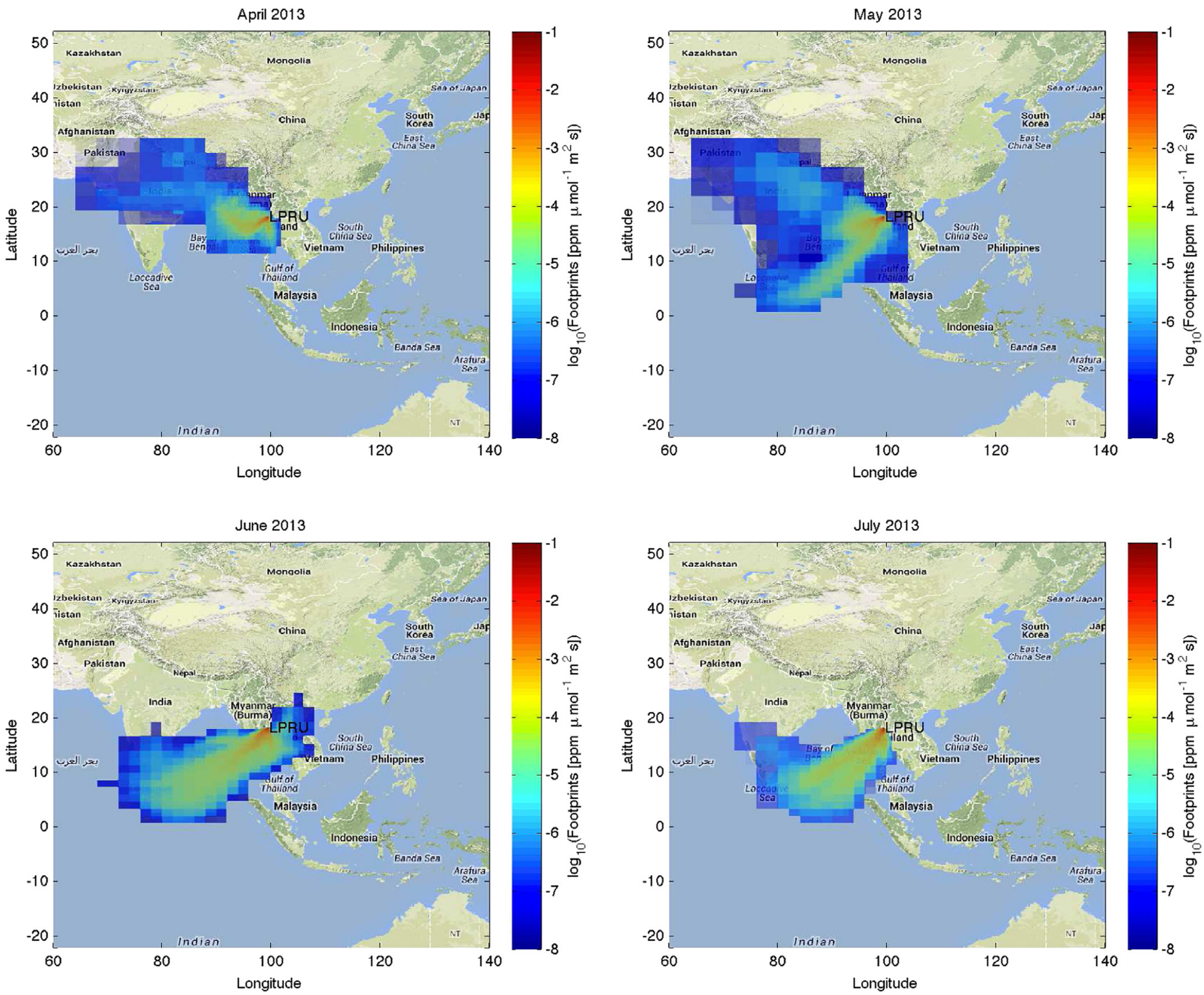

Fig. 9. 3-day backtrajectory footprints for LPRU, Thailand for April, May, June and July 2013.

period of June 18–22, 2013. From June 23–25, 2013, the sea level pressure increased up to 982.5 hPa accompanied by an increase in the surface CO_2 concentration amplitudes. After this period, the sea level pressure decreased to 980 hPa followed by a decrease in surface carbon dioxide concentration amplitudes, but not as low as from June 18–22, 2013.

For the IESM site, the outer bands of a Category 5 typhoon, internationally named Usagi (locally named Odette), passed by the IESM site as shown in Fig. 6. With the lowest pressure of the typhoon at 910 hPa, the passage of Usagi essentially took away the diurnal cycle of surface CO_2 concentrations from September 20–23, 2013.

The independent variable of sea level pressure, x_{i2}, is also associated with the second dominant regression coefficient, β_2, for the LPRU and IESM sites (see Tables 1 and 2).

Other factors, such as the transport of surface CO_2 fluxes to the measurement site, also affect the day-to-day variations in surface carbon dioxide concentrations. These are not considered in the multiple linear regression, hence the RMS errors reported (see Table 2 and Figs. 2 and 3). Using the STILT model, 3-h backtrajectory *footprints* were simulated for each measurement (hourly for LPRU and 3-hourly for IESM) then averaged over a month to infer regions that may influence the measurements. A fixed horizontal resolution of ~1.84 × 2.78 km was utilized for the 3-h backtrajectory footprints. Since the range of the footprints cover more than an order of magnitude, its logarithm was calculated. This is shown in Figs. 7 and 8 for the LPRU and the IESM sites, respectively. Red contour colors represent regions with high influence to the measurements while blue contour colors represent regions with low influence to the measurements.

Transboundary transport was also examined using 3-day backtrajectory footprints simulated at a dynamic horizontal resolution (for efficient computation) with the smallest horizontal resolution being ~18.4 × 27.8 km. These are shown in Figs. 9 and 10 for LPRU and IESM, respectively.

During the measurement period at LPRU, the winds generally come from the southwest. CO_2 sources upwind of the measurement site, such as biomass burning during April, may influence the measurements. In Fig. 7, MODIS fire hotspot data, which are based on brightness temperature, have been overlaid with the footprints.

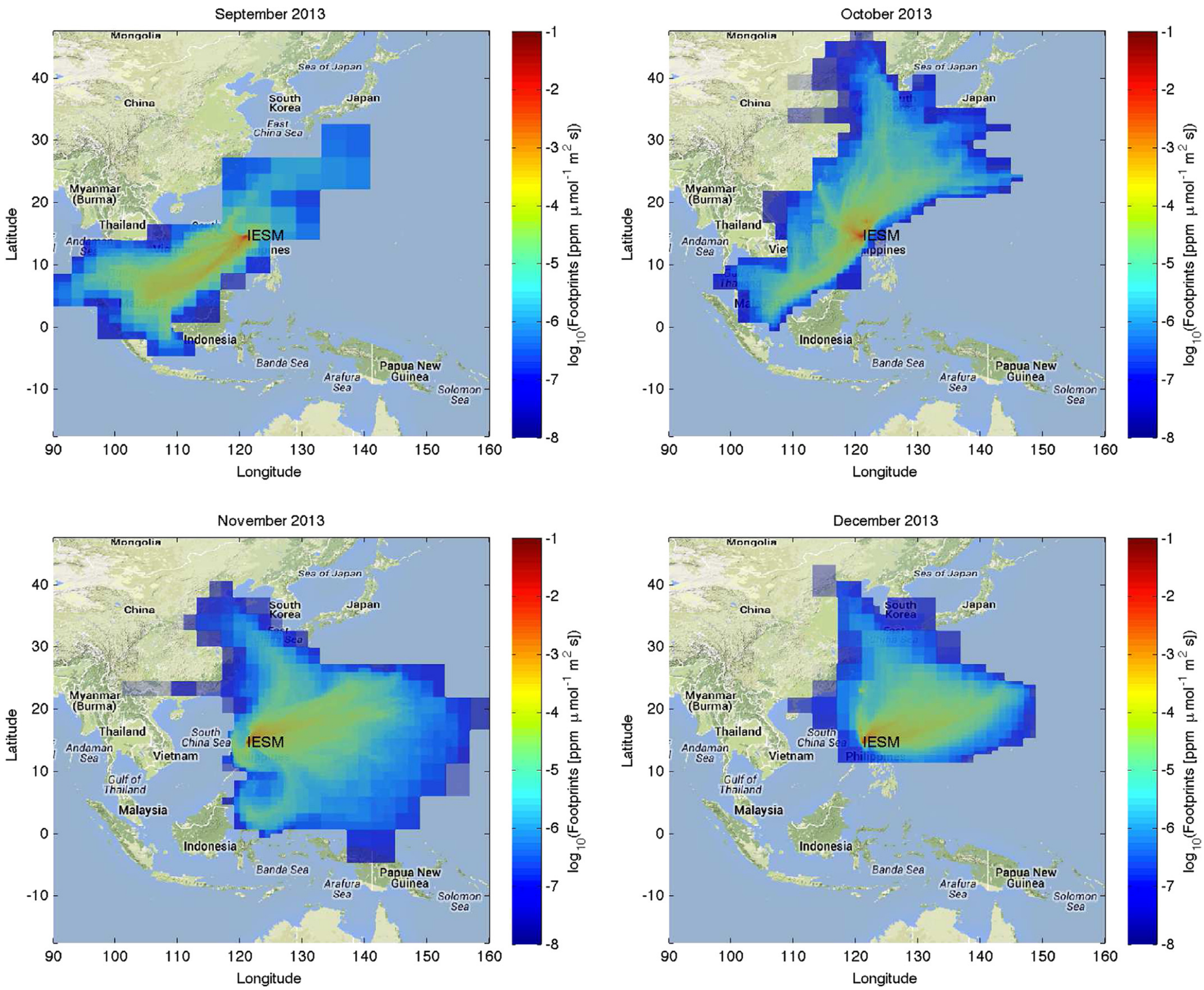

Fig. 10. 3-day backtrajectory footprints for IESM, Philippines for September, October, November and December 2013.

The green stars indicate 0–30% confidence in the fire hotspot data; the yellow stars depict 30–80% confidence; while the red stars represent more than 80% confidence (Justice et al., 2011). This still needs to be further quantified though, and in this study, only a qualitative treatment was done.

At the IESM site, September is generally still part of the southwest monsoon season, October being a monsoon transition phase and November to December belong to the northeast monsoon season. Surrounding the IESM site are several power plants, landfills, dams (which may release CO_2 during outgassing) (Guérin et al., 2006), and volcanic fields which are all potential sources of carbon dioxide.

Complex terrain also surrounds both sites, making topography also a factor in CO_2 entrainment producing regions with high surface carbon dioxide concentrations.

Depending upon the strength of the monsoon, transboundary transport is also a factor in the surface CO_2 concentration variations. This is especially evident at the IESM site particularly during monsoon surges, tropical cyclone enhanced monsoons and typhoons (Typhoon Haiyan occurred in November) as shown in Fig. 10 for the months of September, October and November. Influences may come from as far as Indonesia and China.

5. Conclusion and Recommendations

The contribution of several factors to the surface CO_2 concentrations was assessed. Using multiple linear regression, air temperature and sea level pressure were the primary meteorological contributors to surface CO_2 variations for both sites. Meteorological factors are not enough to explain the variations in surface carbon dioxide. Surface CO_2 flux and transboundary transport should also be considered. In this study, only a qualitative approach was taken in inferring regions that may influence the measurements. The footprints only indicate probable locations where CO_2 sources may occur. More has to be done to exactly pinpoint where these carbon dioxide sources are. Quantifying the contribution of surface CO_2 fluxes to the measurements still has to be performed.

Acknowledgements

The authors would like to thank the Natural Sciences Research Institute of the University of the Philippines as well as Lampang Rajabhat University, Thailand for funding this research. We also would like to extend our gratitude to all those who made this work possible.

References

Gerbig, C., Lin, J.C., Wofsy, S.C., Daube, B.C., Andrews, A.E., Stephens, B.B., Bakwin, P.S., Grainger, C.A., 2003. Toward constraining regional-scale fluxes of CO_2 with atmospheric observations over a continent: 1. Observed spatial variability from airborne platforms. J. Geophys. Res. Atmos. 108 (D24) http://dx.doi.org/10.1029/2002JD003018 n/a–n/a.

Guérin, F., Abril, G., Richard, S., Burban, B., Reynouard, C., Seyler, P., Delmas, R., 2006. Methane and carbon dioxide emissions from tropical reservoirs: significance of downstream rivers. Geophys. Res. Lett. 33 (21), L21407. http://dx.doi.org/10.1029/2006GL027929.

IPCC, Field, C.B., Barros, V., Stocker, T.F., Qin, D., Dokken, D.J., Ebi, K.L., Mastrandrea, M.D., M, K.J., Plattner, G.-K., Allen, S.K., Tignor, M., M, P.M., 2012. In: Field, C.B., Barros, V., Stocker, T.F., Dahe, Q. (Eds.), Managing the Risks of Extreme Events and Disasters to Advance Climate Change Adaptation. Cambridge University Press, Cambridge. http://dx.doi.org/10.1017/CBO9781139177245.

Justice, C.O., Giglio, L., Ramachandran, B., Abrams, M.J., 2011. MODIS-derived Global Fire Products. In: Land Remote Sensing and Global Environmental Change, vol. 11. Springer, New York, pp. 661–679. http://dx.doi.org/10.1007/978-1-4419-6749-7_29.

Kalnay, E., Kanamitsu, M., 1996. The NCEP/NCAR 40-Year reanalysis project. Bull. Am. Meteorol. Soc. 77, 437–470.

Lin, J.C., Gerbig, C., Wofsy, S.C., Andrews, A.E., Daube, B.C., Davis, K.J., Grainger, C.A., 2003. A near-field tool for simulating the upstream influence of atmospheric observations: the Stochastic Time-Inverted Lagrangian Transport (STILT) model. J. Geophys. Res. 108 (D16) http://dx.doi.org/10.1029/2002JD003161. ACH 2-1-ACH 2-17.

Potsdam Institute of Climate Research and Climate Analytics, 2013. Turn Down the Heat. Washington DC.

Stephens, B.B., Gurney, K.R., Tans, P.P., Sweeney, C., Peters, W., Bruhwiler, L., Ciais, P., Ramonet, M., Bousquet, P., Nakazawa, T., Aoki, S., Machida, T., Inoue, G., Vinnichenko, N., Lloyd, J., Jordan, A., Heimann, M., Shibistova, O., Langenfelds, R., Steele, P., Francey, R., Denning, S., 2007. Weak northern and strong tropical land carbon uptake from vertical profiles of atmospheric CO_2. Science (New York, N.Y.) 316 (5832), 1732–1735. http://dx.doi.org/10.1126/science.1137004.